

Expansion of Vortex Cores by Strong Electronic Correlation in $\text{La}_{2-x}\text{Sr}_x\text{CuO}_4$ at Low Magnetic Induction

R. Kadono,^{1,*} W. Higemoto,¹ A. Koda,¹ M. I. Larkin,² G. M. Luke,^{2,†} A.T. Savici,² Y. J. Uemura,² K. M. Kojima,³ T. Okamoto,³ T. Kakeshita,³ S. Uchida,³ T. Ito,⁴ K. Oka,⁴ M. Takigawa,⁵ M. Ichioka,⁵ and K. Machida⁵

¹*Institute of Materials Structure Science, High Energy Accelerator Research Organization (KEK), Tsukuba, Ibaraki 305-0801, Japan*

²*Physics Department, Columbia University, New York, NY10027, USA*

³*Department of Superconductivity, University of Tokyo, Tokyo 113-8656, Japan*

⁴*National Institute of Advanced Industrial Science and Technology, Tsukuba, Ibaraki 305-8562, Japan*

⁵*Department of Physics, Okayama University, Okayama 700-8530, Japan*

(Dated: November 14, 2018)

The vortex core radius ρ_v , defined as the peak position of the supercurrent around the vortex, has been determined by muon spin rotation measurements in the mixed state of $\text{La}_{2-x}\text{Sr}_x\text{CuO}_4$ for $x = 0.13, 0.15$, and 0.19 . At lower doping ($x = 0.13$ and 0.15), $\rho_v(T)$ increases with decreasing temperature T , which is opposite to the behavior predicted by the conventional theory. Moreover, $\rho_v(T \rightarrow 0)$ is significantly larger than the Ginsburg-Landau coherence length determined by the upper critical field, and shows a clear tendency to decrease with increasing the doping x . These features can be qualitatively reproduced in a microscopic model involving antiferromagnetic electronic correlations.

The structural and electronic properties of the flux line lattice (FLL) state in high- T_c cuprates have been extensively studied by microscopic techniques, including scanning tunneling spectroscopy (STS), small angle neutron scattering (SANS), nuclear magnetic resonance (NMR), and muon spin rotation (μSR). Rich information has been provided not only on the superconductivity itself, but also on the unique FLL state as a ‘vortex matter’ realized in $\text{YBa}_2\text{Cu}_3\text{O}_{7-\delta}$ (YBCO) and $\text{Bi}_2\text{Sr}_2\text{CaCu}_2\text{O}_{8+\delta}$ (BSCCO) systems. In particular, recent developments concerning the μSR experimental technique have made it feasible to obtain microscopic details of the spatial field distribution $B(\mathbf{r})$ in the FLL state directly from the μSR time spectra¹. The application of this advanced μSR technique to various type II superconductors including YBCO has revealed that the vortex core radius ρ_v , which must be proportional to the Ginzburg-Landau (GL) coherence length ξ_{GL} near the transition temperature (T_c), strongly depends on the external magnetic field: ρ_v exhibits a sharp increase with decreasing field at lower fields, while it tends to converge to $\xi_{\text{GL}} \equiv \sqrt{\Phi_0/2\pi H_{c2}}$ at higher fields (with Φ_0 and H_{c2} being the flux quantum and the upper critical field, respectively)^{2,3}. This indicates that the conventional picture of the FLL state, in which the vortices are regarded as being simple arrays of rigid cylinders (with a radius ξ_{GL}) containing normal electrons, is valid only near T_c , i.e., the region prerequisite for the application of the GL theory. A recent calculation based on the quasiclassical Eilenberger theory⁴ has successfully reproduced the observed field dependence of ρ_v in CeRu_2 in which an isotropic order parameter is realized for $H/H_{c2} \leq 0.5$ ⁵. On the other hand, the result of a similar calculation for anisotropic d -wave superconductors is far from satisfactory to explain the experimental observation in YBCO, where ρ_v exhibits a much steeper change compared with the theoretical prediction.

Meanwhile, similar studies on the $\text{La}_{2-x}\text{Sr}_x\text{CuO}_4$

(LSCO) system are still in a preliminary stage because both the STS and SANS techniques have rarely been successful in observing vortices in this compound. It is only very recently that the SANS signal from FLL has been reported in an overdoped LSCO with the revelation of a square FLL structure at higher magnetic fields⁶. The previous μSR studies on LSCO were mostly concerned with remnant magnetism over the underdoped region, including that near $x = 1/8$ ⁷, or with magnetic penetration depth, λ , which was evaluated from the total linewidth without any detailed modeling of the microscopic structure of vortices⁸. To our knowledge, there has only been one attempt to derive the vortex core size, which found a relatively large cutoff parameter assuming the modified London model⁹.

In this work, we report on high-precision μSR measurements of the magnetic field distribution in the mixed state of $\text{La}_{2-x}\text{Sr}_x\text{CuO}_4$ single crystals. We found that the field distribution at lower fields ($H < 0.4$ T) is perfectly reproduced by a modified London model with a Lorentzian cutoff. The actual size of ρ_v defined as the peak of the supercurrent density deduced from Maxwell’s relation was quite large (e.g., $\rho_v \simeq 80$ Å for $x = 0.15$), being much larger than ξ_{GL} ($\simeq 23$ Å for $x = 0.15$). More importantly, we have found that i) $\rho_v(T)$ in LSCO with $x = 0.13$ and 0.15 tends to increase with decreasing temperature T , and that ii) $\rho_v(0)$ exhibits a monotonic decrease with increasing doping x . While these features are qualitatively unique compared with YBCO¹⁰ and have no simple explanation within the conventional theoretical model, they can be reproduced in a model involving strong antiferromagnetic correlations competing with superconductivity.

μSR experiments on two sets of single crystalline $\text{La}_{2-x}\text{Sr}_x\text{CuO}_4$ (one with $x = 0.15$, labeled LA15, and those with $x = 0.13, 0.15$, and 0.19 , labeled LB13, LB15, and LB19, respectively) were performed on the M15

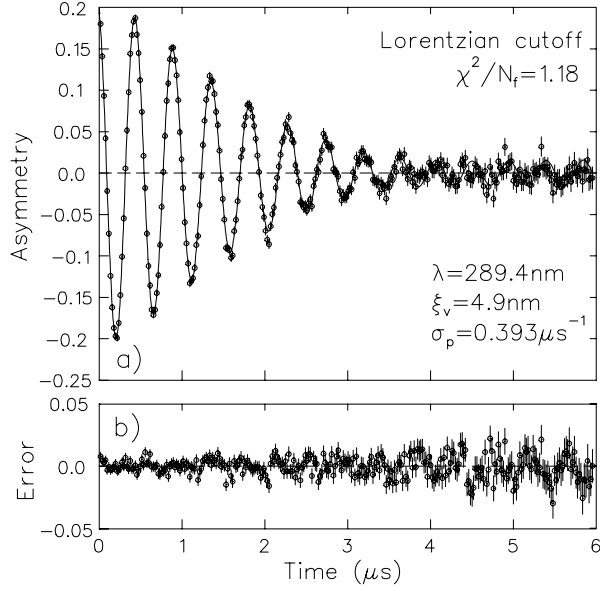


FIG. 1: a) Time differential μ - e decay asymmetry in $\text{La}_{1.85}\text{Sr}_{0.15}\text{CuO}_4$ (LA15) at 15 K and $H = 0.2$ T, where the solid curve shows the result of a fitting analysis with a Lorentzian cutoff (see text). b) Difference between the data and the solid curve, which is defined as the error of the fitting analysis.

beamline at the TRIUMF muon facility which provides a beam of nearly 100% spin-polarized positive muons of momentum 29 MeV/c. Some results on LB15 were previously reported⁹. The specimen was loaded onto a He-flow cryostat and cooled from a temperature above T_c after setting the magnetic field at every field point (i.e., field-cooling) to minimize the effect of flux pinning. The initial muon spin polarization was perpendicular to the magnetic field H , and thus to the FLL in the superconducting state, as the crystal c -axis was aligned parallel to H so that the field distribution associated with the FLL was determined by the in-plane penetration depth λ_{ab} and the coherence length ξ_{ab} . In zero field, μ SR results from the specimen LA15 exhibited slightly enhanced spin relaxation below ~ 10 K, which was virtually absent in LB15. The spin relaxation rate in LA15 at 3.5 K was greater than that at 41 K by $0.026(2) \mu\text{s}^{-1}$, indicating a weak remnant magnetism. In addition, we observed an additional component undergoing a fast spin relaxation in LA15 in measurements with an applied field above 0.4 T, which became more prominent at higher fields. In the present study, we analyzed data obtained only for $H = 0.2$ T which do not exhibit such additional relaxation, in order to avoid any complication due to magnetism. We will report on high-field μ SR measurements in all of these specimens in a separate paper¹¹, and discuss the possible relation to field-induced magnetism suggested by neutron diffraction^{12,13,14}.

Since muons stop randomly along the length scale of FLL, the time evolution of complex muon polarization $\hat{P}(t)$ provides a random sampling of the internal field

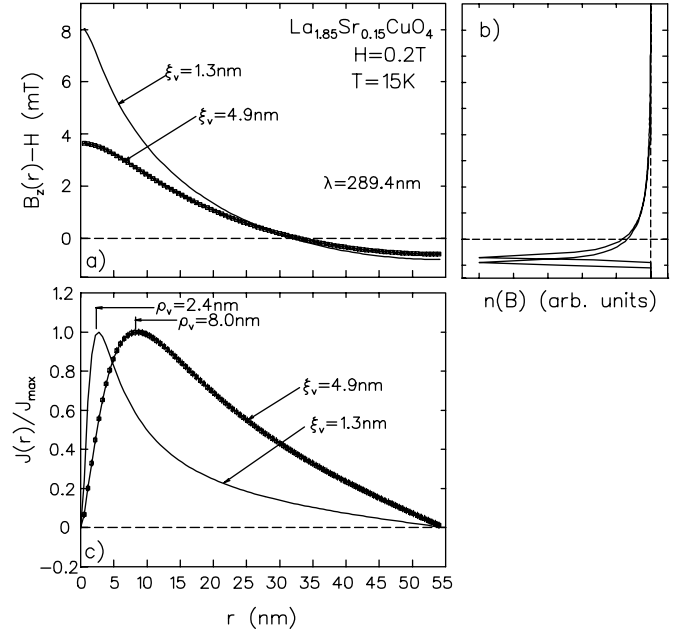


FIG. 2: a) Example of the reconstructed field distribution ($B_z(r)$, solid line with data shown by open squares) using the result of Fig. 1, which yields the spectral density ($n(B)$) in b). The radial distribution of the supercurrent density, $J(r) = |\text{rot}\mathbf{B}(\mathbf{r})|$, is shown in c) along with a definition of the core radius ρ_v . For a comparison, those corresponding to $\rho_v = \xi_{\text{GL}}$ are also displayed.

distribution, $\mathbf{B}(\mathbf{r}) = (0, 0, B(\mathbf{r}))$,

$$\begin{aligned} \hat{P}(t) &\equiv P_x(t) + iP_y(t) \\ &= \exp(-\sigma_p^2 t^2) \int_{-\infty}^{\infty} n(B) \exp(i\gamma_\mu B t - i\psi) dB, \end{aligned} \quad (1)$$

$$n(B) = \langle \delta(B - B(\mathbf{r})) \rangle_{\mathbf{r}}, \quad (2)$$

where $P_{x,y}(t)$ is proportional to the time-dependent μ^+ - e^+ decay asymmetry $A_{x,y}(t)$ deduced from the corresponding sets of positron counters $N_\psi(t)$ ($\psi = n\pi/2$, with $n = 0, 2$ and $1, 3$) after subtracting constant backgrounds estimated from data at earlier times ($t < 0$),

$$A_x(t) = N_0(t)/N_\pi(t) = A_0 P_x(t), \quad (3)$$

$$A_y(t) = \alpha N_{\pi/2}(t)/N_{3\pi/2}(t) = A_0 P_y(t), \quad (4)$$

with $\alpha = [N_0(0)N_{3\pi/2}(0)]/[N_\pi(0)N_{\pi/2}(0)]$, A_0 is the normalized instrumental asymmetry, σ_p is the additional relaxation due to random flux pinning, $n(B)$ is the spectral density for the internal field defined as a spatial average ($\langle \rangle_{\mathbf{r}}$) of the delta function, γ_μ is the muon gyromagnetic ratio ($= 2\pi \times 135.53$ MHz/T), and ψ is the initial phase¹⁵. These equations indicate that the real amplitude of the Fourier-transformed muon precession signal corresponds to $n(B)$ with an appropriate correction of σ_p . In the modified London model, $B(\mathbf{r})$ is approximated as the sum of the magnetic induction from isolated vortices to yield

$$B(\mathbf{r}) = B_0 \sum_{\mathbf{K}} \frac{e^{-i\mathbf{K}\cdot\mathbf{r}}}{1 + K^2 \lambda^2} F(K, \xi_v), \quad (5)$$

where \mathbf{K} are the vortex reciprocal lattice vectors, B_0 ($\simeq H$) is the average internal field, λ is the London penetration depth, and $F(K, \xi_v)$ is a nonlocal correction term with ξ_v being the cutoff parameter for the magnetic field distribution; it must be stressed that ξ_v is a parameter to describe the electromagnetic response of a vortex, thereby not necessarily equivalent to the core radius ρ_v . Considering small anisotropy predicted by the theory⁴, we assumed an isotropic vortex core and associated field distribution near the vortex center.

TABLE I: A comparison of the central field between points above and below the superconducting transition temperature T_c , where the external field was set to 6 T above T_c and then field-cooled. The relative precision of the field ($|\Delta f/f|$) was better than 10^{-4} for all cases. Note that the effect of field inhomogeneity and/or the Knight shift is larger at higher fields. Therefore, the above number gives an upper bound for the uncertainty of the central field.

Samples	$f = \gamma_\mu B_0 / 2\pi$ (MHz)		$ \Delta f/f $
	$T > T_c$	$T < 4$ K ($\ll T_c$)	
LA15	812.9905(22)	812.9902(66)	$0.0(9) \times 10^{-5}$
LB13	813.0765(15)	813.0533(41)	$2.9(5) \times 10^{-5}$
LB15	812.8405(17)	812.7686(30)	$8.9(3) \times 10^{-5}$
LB19	813.0679(12)	813.0384(19)	$3.6(3) \times 10^{-5}$

As summarized in Table I, the relative change of B_0 due to field inhomogeneity and/or the Knight shift was less than 10^{-4} throughout measurements below 50 K, and therefore B_0 was fixed to the value determined in the normal state ($T > T_c$) for the analysis of data below T_c . This well-defined B_0 , together with the strongly asymmetric feature of $n(B)$ against B_0 , allowed us to deduce the physical parameters including λ and ξ_v without much ambiguity. Moreover, we have found that the deduced values of ξ_v (and thereby ρ_v) were virtually independent of the apex angle (θ) of FLL, while λ showed a considerable dependence on θ . This feature can be readily understood by considering the fact that the change in the apex angle has least effect on the field distribution of single vortex near the center (corresponding to the high-field end of $n(B)$), while it does modify the overlap of field distribution between the vortices. Based on this robustness of the analysis result against θ , we assumed triangular FLL ($\theta = \pi/3$) throughout the following data analysis for simplicity. We have also found that the μ SR spectra in LSCO at lower fields are much better reproduced by the Lorentzian cutoff, $F(K, \xi_v) = \exp(-\sqrt{2}K\xi_v)$, compared with the conventional Gaussian cutoff, $F(K, \xi_v) = \exp(-K^2\xi_v^2/2)$. Figure 1 shows a typical example of the measured decay asymmetry, $A_x(t) (\propto P_x(t))$, observed at 0.2 T in specimen LA15 together with the result of a fitting analysis. The reduced chi-square χ^2/N_f (where N_f denotes the number of degrees of freedom) is close to the ideal value of $\simeq 1$ when the Lorentzian cutoff is applied to Eq. (5), while it becomes much worse as $\chi^2/N_f \simeq 1.61$

with the Gaussian cutoff. A similar tendency was commonly observed in all other samples. This observation is consistent with the result of a theoretical analysis which showed that the Lorentzian cutoff is indeed a better approximation at the low-field limit^{16,17}. Accordingly, all of the μ SR time spectra were analyzed by comparing the data with the time evolution calculated by Eqs. (1)~(5) using the Lorentzian cutoff, where A_0 , ψ , σ_p , ξ_v , and λ were free parameters while B_0 and θ were always fixed.

While the fitting analysis of the μ SR data is performed entirely in time domain, one can reconstruct $B(\mathbf{r})$ by Eq.(5) using the physical parameters deduced from the fitting analysis. An example of the reconstructed field distribution, $B(\mathbf{r}) = B_z(r)$, along the radial direction from the core center to a saddle point is shown in Fig. 2a, together with the corresponding $n(B)$ (Fig. 2b) and supercurrent density, $J(r) = |\text{rot}\mathbf{B}(\mathbf{r})|$ (Fig. 2c). As shown in Fig. 2c, the core radius defined by $J(\rho_v) = J_{\text{max}}$ (where J_{max} denotes the maximum of $J(r)$) is considerably larger than the magnetic cutoff parameter ξ_v , indicating the need for a special precaution in interpreting ξ_v directly as the core radius. However, the result of a data analysis for various fields/temperatures indicates that ρ_v is always proportional to ξ_v . It has been estimated that $\xi_{\text{GL}} \simeq 23$ Å for an optimally doped sample ($H_{c2} \simeq 62$ T for $x = 0.15$ ¹⁸). Provided that ρ_v is independent of the field and determined by ξ_{GL} (i.e., $\rho_v \simeq 0.6 \sim 0.8\xi_{\text{GL}}$ as predicted by theory⁴), then ξ_v must be smaller than 13 Å to reproduce the corresponding core radius (see Fig. 2). However, an attempt to fit the data assuming $\xi_v = 13$ Å completely fails to reproduce the data; the reduced chi-square χ^2/N_f was 2.76 at its best when other parameters (i.e., A_0 , ψ , σ_p , and λ) were set free to minimize χ^2/N_f . This is primarily because, as evident in Fig. 2b, the peak of $n(B)$ shifts significantly to a lower field, which cannot be compensated by any other parameters within the current model. Note that B_0 is determined with a relative precision better than $\times 10^{-4}$ so that the shift of the peak in Fig. 2b ($\simeq 0.2$ mT) is readily discernible. Thus, it is inferred from these results that ρ_v is about three times as large as ξ_{GL} near the lower critical field. This tendency is qualitatively in line with the theoretical prediction, although the magnitude is yet to be explained⁴.

The deduced vortex core radius for samples LB13, LB15, and LB19, as a function of the temperature, are shown in Figs. 3a-c together with the results for LA15. It exhibits a slight increase with decreasing temperature for $x = 0.13$ and 0.15, while an opposite tendency is observed for $x = 0.19$. No such anomaly has been reported for YBCO¹⁰. Note that the conventional theory^{19,20} predicts a behavior opposite to what is actually observed in the former cases (see Fig. 3d). The values deduced from the data in LA15 are in good agreement with those in LB15, indicating that the influence of the remnant magnetism found in LA15 is not significant at $H = 0.2$ T and $T \geq 15$ K. The penetration depth extrapolated to 0 K was 2559(50) Å in LA15, 2446(6) Å, 2460(4) Å, and 2051(7) Å in LB13, LB15, and LB19, respectively. The

relatively large error for LA15 is due to the influence of the remnant magnetism below 10 K. We also note that σ_p was typically $0.4\sim 0.5 \mu\text{s}^{-1}$ at the lowest temperature in all specimens, showing a common tendency of gradual decrease with increasing temperature. This is understood as the thermal depinning of FLL from random pinning centers.

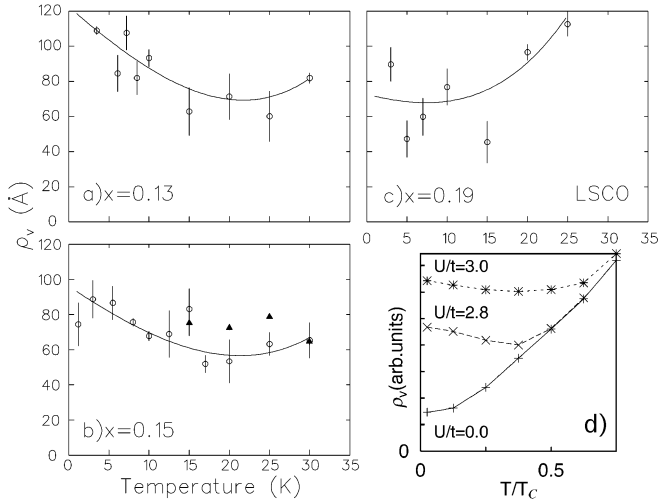


FIG. 3: Temperature dependence of the vortex core radius at $H = 0.2$ T for specimens a) LB13, b) LA15 (triangles) and LB15, and c) LB19. d) Calculated ρ_v vs T/T_c using the model in Ref.²¹, where U/t represents the strength of the electronic correlation (T_c is the superconducting transition temperature). The solid curves in a)-c) show fitting results by an analytical approximation of d) to deduce the extrapolated values $\rho_v(0)$.

For understanding the T -dependence of ρ_v , we performed a model calculation based on Bogoliubov-de Gennes theory, where both the d -wave superconductivity and the spatially modulated antiferromagnetic (AF) spin correlations are simultaneously considered by incorporating a pairing interaction to the standard Hubbard model for two-dimensional square lattice²¹. As can be seen in Fig. 3d, the core radius at which the superconducting order parameter reaches 60 % of the bulk value, is strongly enhanced when the electronic correlation is present (i.e., $U/t > 0$, with U and t being the respective on-site Coulomb energy and transfer matrix element to the nearest neighboring sites in the Hubbard model), while it obeys the prediction by Kramer and Pesch when $U/t = 0$ ^{19,20}. The T -dependence of ρ_v for $U/t > 0$ qualitatively agrees with those observed for $x = 0.13$ and 0.15 . In the model, this feature is due to AF spin correlations induced at the core sites, leading to a reduction of the local pairing amplitude and an associated increase of ρ_v at lower temperatures. The absence of quasistatic antiferromagnetism may be explained by the strongly dynamical spin fluctuations in the relevant field/temperature range.

In order to obtain the extrapolated value $\rho_v(0)$, the data in Figs. 3a-3c were analyzed by the χ^2 -minimization

TABLE II: Parameter values for Eq. (6) deduced by fitting data in Fig. 3a-3c.

Samples	$\rho_v(0)$ (Å)	c_1	c_2	c_3	χ^2/N_f
LB13	120.9 (4.6)	-6.36(3)	-2.69(4)	2.65(2)	7.5/5
LB15	95.0(7.3)	-6.42(5)	-2.68(6)	2.72(4)	9.8/7
LB19	73.3(11.5)	-5.51(6)	-2.14(9)	2.91(4)	18.5/3

method using an analytical approximation of Fig. 3d,

$$\rho_v(\bar{T}) = \rho_v(0) \{1 + c_1(\bar{T}) + c_2(\exp(-\bar{T}) - 1) + c_3(\exp(\bar{T}) - 1)\} \quad (6)$$

under a condition $c_1 < c_2 < 0 < c_3$ with $\bar{T} = T/T_c$. The result of fitting analysis is summarized in Table II. The values of $\rho_v(0)$ are plotted against the Sr concentration x in Fig. 4. (The data of LA15 were not used for this analysis because they were available only for $T \geq 15$ K, leading to large uncertainty in the fitting.) As the hole doping progresses with increasing x , the core size decreases monotonically. We note that almost equivalent result was obtained by an independent analysis using a linear function $\rho_v(\bar{T}) = \rho_v(0)(1 + c\bar{T})$ for $T < 0.5T_c$. We shall compare this behavior with those of other relevant parameters. Firstly, $\rho_v(0)$ and T_c have no simple correlations, since T_c shows a maximum at $x = 0.15$. Secondly, the superconducting gap, Δ , does not scale with $\rho_v(0)$, if Δ scales with T_c . In contrast, $\rho_v(0)$ in YBCO is larger for the lower T_c , thus following the simple scaling law¹⁰. It has been noticed in LSCO that the gap (or pseudo-gap) increases with decreasing hole concentration in the optimum-to-underdoped region. In this sense, the (pseudo-) gap value and $\rho_v(0)$ vary along with each other. This behavior is opposite to that expected in a simple BCS superconductor, where the coherence length is inversely proportional to the gap value as $\xi_0 = \hbar v_F / \pi \Delta$, where v_F denotes the Fermi velocity. In $\text{La}_{2-x}\text{Sr}_x\text{CuO}_4$, the Fermi velocity has been known to have little dependence on x . It is interesting to note that the model calculation shown in Fig. 3d appears to simulate the doping dependence if we assume that the incipient AF correlations become weaker ($U/t \rightarrow 0$) as the doping proceeds. A similar result has been reported for the correlation length, $\xi_{\text{Zn}}(x)$, in Zn-doped $\text{La}_{2-x}\text{Sr}_x\text{CuO}_4$ over which the pairing is suppressed²².

Finally, we point out the potential link between our results and those of recent neutron scattering in LSCO where a field-induced quasistatic antiferromagnetism has been suggested^{12,13,14}. Although it has not been clearly identified as being due to the vortex cores, they found that a long-range AF correlation is recovered in the mixed state under moderate magnetic fields of a few Tesla. A similar situation is also suggested in YBCO^{23,24}, BSCCO²⁵, and $\text{YBa}_2\text{Cu}_4\text{O}_8$ ²⁶. The enhanced vortex core radius at lower fields in LSCO may be interpreted as a precursor of such a quasistatic correlation. Besides our model calculation, theories including those based on the t - J model^{27,28} or $\text{SO}(5)$ symmetry²⁹ also predict the de-

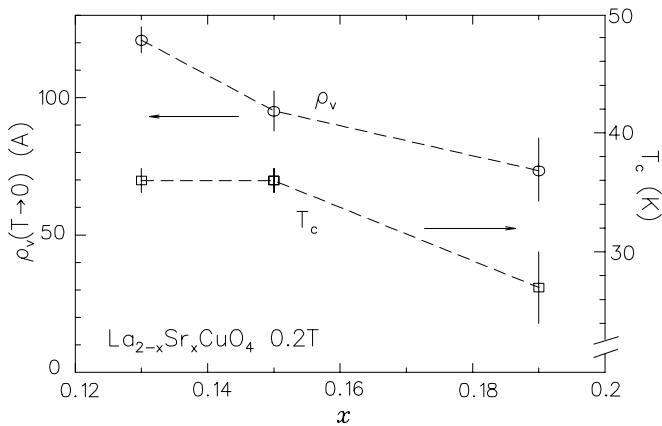


FIG. 4: Doping dependence of ρ_v extrapolated to 0 K at $H = 0.2$ T and that of the superconducting transition temperature (T_c) determined by the Meissner effect. The lines are guides for the eye.

velopment of AF correlations in place of a superconducting order parameter when the latter is suppressed by a

magnetic field or impurity atoms. When the superconducting order parameter is suppressed at the center of vortices, one would expect the emergence of AF spin correlations around the vortex cores, which may be strongly dynamical at lower fields.

In summary, we have found in LSCO that the vortex core radius at 0.2 T is about three times as large as that estimated from H_{c2} . The core size increases monotonically with decreasing Sr doping with an unusual temperature dependence for $x = 0.13$ and 0.15. Compared with the cases of other cuprates, these features more strongly suggest a possibility that ρ_v is influenced by the two-dimensional AF correlations in this system.

We would like to thank the staff of TRIUMF for their technical support during the experiment. This work was partially supported by a Grant-in-Aid for Scientific Research on Priority Areas and a Grant-in-Aid for Creative Scientific Research from the Ministry of Education, Culture, Sports, Science and Technology of Japan, NSF Grand DMR-01-02752 and CHE-01-17752 at Columbia, and by NSERC of Canada.

* Also at School of Mathematical and Physical Science, The Graduate University for Advanced Studies

† Present address: Department of Physics and Astronomy, McMaster University, Hamilton, ON L8P4N3, Canada

¹ For a recent review, see, for example, J. E. Sonier, J. H. Brewer, and R. F. Kiefl, *Rev. Mod. Phys.* **72**, 769 (2000).

² J. E. Sonier, J. H. Brewer, R. F. Kiefl, G. D. Morris, R. I. Miller, D. A. Bonn, J. Chakhalian, R. H. Heffner, W. N. Hardy, and R. Liang, *Phys. Rev. Lett.* **83**, 4156 (1999).

³ K. Ohishi, K. Kakuta, J. Akimitsu, W. Higemoto, R. Kadono, J.E. Sonier, A.N. Price, R.I. Miller, R.F. Kiefl, M. Nohara, H. Suzuki and H. Takagi, *Phys. Rev. B* **65**, 140505 (2002).

⁴ M. Ichioka, A. Hasegawa, and K. Machida, *Phys. Rev. B* **59**, 184 (1999).

⁵ R. Kadono, W. Higemoto, A. Koda, K. Ohishi, T. Yokoo, J. Akimitsu, M. Hedo, Y. Inada, Y. Onuki, E. Yamamoto, and Y. Haga, *Phys. Rev. B* **63**, 224520 (2001).

⁶ R. Gilardi, J. Mesot, A. Drew, U. Divakar, S. L. Lee, E. M. Forgan, O. Zaharko, K. Conder, V. K. Aswal, C. D. Dewhurst, R. Cubitt, N. Momono, and M. Oda, *Phys. Rev. Lett.* **88**, 217003 (2002).

⁷ I. Watanabe, K. Nishiyama, K. Nagamine, K. Kawano, and K. Kumagai, *Hyperfine Interact.* **86**, 603 (1994).

⁸ G. Aeppli, R.J. Cava, E.J. Ansaldo, J.H. Brewer, S.R. Kretzmann, G.M. Luke, D.R. Noakes, and R.F. Kiefl, *Phys. Rev. B* **35**, 7129 (1987).

⁹ G. M. Luke, Y. Fudamoto, K. Kojima, M. Larkin, B. Nachumi, Y. J. Uemura, J. E. Sonier, T. Ito, K. Oka, M. de Andrade, M. B. Maple, and S. Uchida, *Physica C* **282-287**, 1465 (1997).

¹⁰ J. E. Sonier, R. F. Kiefl, J. H. Brewer, D. A. Bonn, S. R. Dunsiger, W. N. Hardy, R. Liang, and R. I. Miller, *Phys. Rev. B* **59**, R729 (1999).

¹¹ A. Savici *et al.*, to be published.

¹² S. Katano, M. Sato, K. Yamada, T. Suzuki, and T. Fukase, *Phys. Rev. B* **62**, R14677 (2000).

¹³ B. Lake, G. Aeppli, K. N. Clausen, D. F. McMorrow, K. Lefmann, N. E. Hussey, N. Mangkorntong, M. Nohara, H. Takagi, T. E. Mason, and A. Schröder, *Science* **291**, 1759 (2001).

¹⁴ B. Lake, H. M. Ronnow, N. B. Christensen, G. Aeppli, K. Lefmann, D. F. McMorrow, P. Vorderwisch, P. Smeibidl, N. Mangkorntong, T. Sasagawa, M. Nohara, H. Takagi, and T. E. Mason, *Nature* **415**, 299 (2002).

¹⁵ E. H. Brandt, *J. Low Temp. Phys.* **73**, 355 (1988).

¹⁶ J. R. Clem, *J. Low Temp. Phys.* **18**, 427 (1975).

¹⁷ A. Yaouanc, P. Dalmas de Réotier, and E. H. Brandt, *Phys. Rev. B* **55**, 11107 (1997).

¹⁸ Y. Ando, G. S. Boebinger, A. Passner, L. F. Schneemeyer, T. Kimura, M. Okuya, S. Watauchi, J. Shimoyama, K. Kishio, K. Tamasaku, N. Ichikawa, and S. Uchida, *Phys. Rev. B* **60**, 12475 (1999).

¹⁹ L. Kramer and W. Pesch, *Z. Phys.* **269**, 59 (1974).

²⁰ N. Hayashi, T. Isoshima, M. Ichioka, and K. Machida, *Phys. Rev. Lett.* **80**, 2921 (1998).

²¹ M. Takigawa, M. Ichioka, and K. Machida, *Phys. Rev. Lett.* **90**, 047001 (2003).

²² T. Nakano, N. Momono, T. Nagata, M. Oda, and M. Ido, *Phys. Rev. B* **58**, 5831 (1998).

²³ V. F. Mitrović, E. E. Sigmund, M. Eschring, H. N. Bachman, W. P. Halperin, A. P. Reyes, P. Kuhns, and W. G. Moulton, *Nature* **413**, 501 (2001).

²⁴ R. I. Miller, R. F. Kiefl, J. H. Brewer, J. E. Sonier, J. Chakhalian, S. Dunsiger, G. D. Morris, A. N. Price, D. A. Bonn, W. H. Hardy, and R. Liang, *Phys. Rev. Lett.* **88**, 137002 (2002).

²⁵ J.E. Hoffman, E.W. Hudson, K.M. Lang, V. Madhavan, S.H. Pan, H. Eisaki, S. Uchida, and J.C. Davis, *Science* **295**, 466 (2002).

²⁶ K. Kakuyanagi, K. Kumagai, and Y. Matsuda, Phys. Rev. B **65**, 60503 (2002).

²⁷ M. Ogata, Int. J. Mod. Phys. B **13**, 3560 (1999).

²⁸ M. Ogata, private communication.

²⁹ S. C. Zhang, Science **275**, 1089 (1997).